BNL-207856-2018-JAAM

Reversible Electrochemical Lithium Ion Insertion into the Rhenium Cluster Chalcogenide-Halide, Re 6 Se 8 Cl 2

A. M. Bruck, X. Tong

To be published in "INORGANIC CHEMISTRY"

May 2018

Center for Functional Nanomaterials

Brookhaven National Laboratory

U.S. Department of Energy

USDOE Office of Science (SC), Basic Energy Sciences (BES) (SC-22)

DISCLAIMER

Reversible Electrochemical Lithium Ion Insertion into the Rhenium Cluster Chalcogenide-Halide, $Re_6Se_8Cl_2$

Andrea M. Bruck[†], Jiefu Yin[†], Xiao Tong[‡], Esther S. Takeuchi[†,||,|], Kenneth J. Takeuchi[†,||], Lisa F. Szczepura[§,*], Amy C. Marschilok[†,||,*]

[†]Department of Chemistry, Stony Brook University, Stony Brook, NY 11794, USA
[‡]Center for Functional Nanomaterials, Brookhaven National Laboratory, Upton, NY 11973, USA
[||]Department of Materials Science and Engineering, Stony Brook University, Stony Brook, NY 11794, USA
[|]Energy Sciences Directorate, Brookhaven National Laboratory, Upton, NY 11973, USA
[§]Department of Chemistry, Illinois State University, Normal, IL, 61790-4160, USA
Supporting Information Placeholder

ABSTRACT: The cluster-based material, $Re_6Se_8Cl_2$, is a two dimensional ternary material with cluster-cluster bonding across the *a* and *b* axes capable of multiple electron transfer accompanied by ion insertion across the *c* axis. The $Li/Re_6Se_8Cl_2$ system showed reversible electron transfer from 1-3 electron equivalents (ee) at high current densities (88 mA/g). Upon cycling to 4 ee, there was evidence of capacity degradation over 50 cycles associated with formation of an organic solid-electrolyte interface (between 1.45-1 V vs. Li/Li^+). This investigation highlights the ability of cluster-based materials with two-dimensional cluster bonding to be used in applications such as energy storage, showing structural stability and high rate capability.

Metal chalcogenides have been identified as high interest materials for energy storage, electronics, optoelectronics, and catalysis.[1,2] Recently, there has been a heightened interest in exploring how changing the dimensionality of metal chalcogenides exploits unique electrical and optical properties that evolve from a changing electronic structure and the accompanying surface effects.[3] To expand on the current understanding of the electronic structure of metal chalcogenides, $Re_6Se_8Cl_2$, from the family of hexarhenium cores $[Re_6Q_{4+n}X_{4-n}]^{(6-n)+}$ (where Q = chalcogen and X = halogen, n = 0-4)[4], was investigated in respect to its ability to function for reversible electrochemical energy storage in a lithium based system.

Previous studies focused on the luminescent and electrochemical properties of the molecular unit $[Re_6Se_8]^{2+}$ with a variety of terminal ligands shown to tune the properties of the electron rich cluster,[5-13] as well as using the cluster core as a building block to prepare materials for a variety of applications.[14-18] This investigation focuses on $Re_6Se_8Cl_2$ with the $[Re_6Se_8]^{2+}$ cluster unit isostructural to that found in the superconducting Mo_6Q_8 Chevrel phase core.[19] Theoretical and experimental studies have explored the ability of Chevrel phase materials (Mo_6S_8) to reversibly transfer 4 electron equivalents (ee) per formula unit.[20-22] Unlike the molybdenum analog, the hexarhenium core has been studied as a "building unit" in extended solid frameworks where motifs of three, two, and single dimensionality are possible.[23,24] These frameworks consists of rigid cluster-cluster linkages, some of which can undergo dimensional reduction in the presence of Cs^+ or Tl^+ halides. These 2D cluster frameworks should be considered as a new class of potential electroactive materials based on this rigid cluster-cluster bonding. Herein, we use $Re_6Se_8Cl_2$ as a model material to illustrate the potential of these frameworks to exhibit multiple electron transfers by electrochemical Li^+ insertion and extraction.

The structure of the two dimensional $Re_6Se_8Cl_2$ contains layers of $[Re_6Se_8]^{2+}$ cores linked by Re_2Se_2 rhombic interactions (along the *a* and *b* axes).[25,26] Each cluster core also contains two terminal chloride ligands arranged in a *trans* fashion creating 2D layers that are only connected by van der Waals interactions. The following formulation, $[Re_6Se^{i}_4Se^{i-a}_{4/2}]Se^{a-i}_{4/2}Cl^{a}_2$ where *i* indicates the inner and *a* the outer (ausser) portions of a single core within the structure (Fig. S1) best describes the repeat pattern in the solid.[25,26]

Synchrotron X-ray Power Diffraction (XPD) confirmed the purity and structure of the material. The as-synthesized $Re_6Se_8Cl_2$ has a triclinic crystal structure with the space group P-1 with unit cell parameters that correspond well to the previously reported structure.[26] In Figure 1, the observed pattern and the corresponding refinement are shown with the crystal structure as the inset with the full refinement parameters provided in Table S1. The most prominent reflection at $2\theta = 1.29^\circ$ (d = 8.13 Å) corresponds to the interlayer distances between clusters. The van der Waals interactions between the terminal chloride ligands (which is described in more detail in Figure S2) leads to the large interlayer spacing. Due to the weak interactions of Cl^- in its local environment and the large distances between atoms in the interlayer spacing it can be envisioned that this material provides adequate channels for Li^+ insertion during electrochemical reduction.

The electrochemistry in a lithium ion based system was explored using cyclic voltammetry (CV) at a slow scan rate of 0.01 mV/s as shown in Figure 2A. The first reduction peak is at 1.72 V with the second at 1.47 V. Quasi reversible electrochemistry is observed with oxidation peaks at 1.98 and 1.79 V. However, at voltages below ~1.3 V during reduction there is a substantial increase in current indicative of side reactions

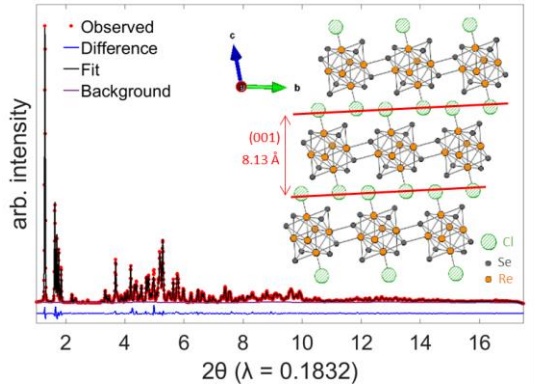

Figure 1: Observed XPD pattern with Rietveld refinement of pristine $Re_6Se_8Cl_2$. The inset is the crystal structure with the (001) plane identified.

occurring until the 1 V limit, consistent with prior reports for lithium based electrochemical cells.[27] Since this large oxidation occurred, CV was also tested with a 1.45 V cut-off voltage with little variation to the corresponding oxidation peaks.

Li-ion half cells were also cycled galvanostatically at the 1 V limit and at a higher voltage limit of 1.45 V. When cycled with a 1.45 V cut-off voltage the first reduction cycle at a rate of 4.4 mA/g yielded 3.1 ee (Fig. S3) which decreased to 2.4 ee by cycle 5 as shown by Figure 2B (where 1 ee = 11.9 mAh/g). At a high rate of 88 mA/g, reversibility of approximately 1.6 ee with the 1.45 voltage cut-off was observed. After cycling to the 1.45 V cut-off the redox profiles at each rate shows little to no variation after 25 cycles (Fig. 2C). The plateau observed during reduction is at approximately 1.7 V with the corresponding oxidation plateau at approximately 2.0 V which correlates well to the CV and shows good reversibility. When cycled to a lower voltage cut-off of 1.0 V, the first reduction (Fig. S4) is well above 15 ee indicating the occurrence of side reactions. This large excess of electron reduction is not reversible upon oxidation as indicated by the Coulombic efficiency of ~26%. The hysteresis between reduction and oxidation reversibly decreased from a 10 electron difference on the first cycle to < 1 electron difference on the fifth cycle at a rate of 4.4 mA/g as shown in Figure 2B. Also, during the fifth cycle the reduction capacity has decreased to 4.8 ee with 4.2 reversible ee in the oxidation process. Increasing the current density to 22, 44, and 88 mA/g appears to suppress the oxidation/reduction hysteresis by inhibiting large amounts of side reactions from occurring where at cycle 20 (at a rate of 88 mA/g, Fig. 2B) the redox capacities are 2.9 and 2.8 ee with less than 0.1 ee hysteresis. At 22, 44, and 88 mA/g the Coulombic efficiencies are all >90% and the reversible ee are ~3.7, 3.2, and 2.8, respectively.

With the lower voltage limit of 1 V the reduction profile shown in Figure 2D at various rates shows a new plateau appear from 2.0 - 1.8 V. This new plateau was not observed in the higher voltage cut-off reactions and is therefore associated with the side reactions occurring below 1.45 V. At a rate of 4.4 mA/g this plateau contributes up to 1 ee of capacity to the reduction process which explains the elevated hysteresis between reduction and oxidation capacity at the slow rates. Interestingly, as the rate increases up to 88 mA/g the voltage plateau at 2.0 V becomes suppressed and does not significantly contribute to the reduction capacity. The effect of rate on the electrochemical properties can be clearly identified by the increasing Columbic efficiency from 87.3% for

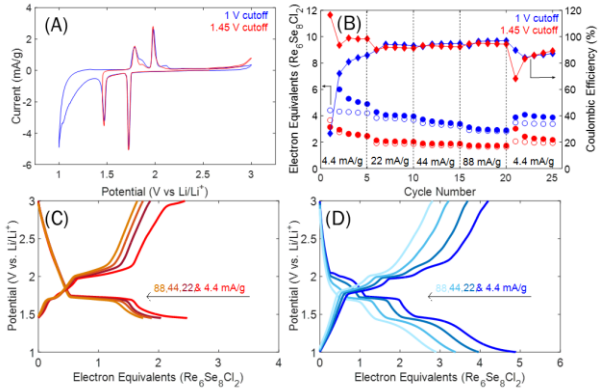

Figure 2: $Li/Re_6Se_8Cl_2$ coin cells (A) CV at a rate of 0.01 mV/s for 1 cycle from 1-3 and 1.45-3 V vs. Li/Li^+. Galvanostatic cycling (B) rate capability test with corresponding coulombic efficiencies and (C-D) voltage profiles at various rates with (C) a 1.45 V and (D) 1 V cut-off voltage. (C-D) voltage profiles correspond to cycles 5, 10, 15, and 20 in (B). Cycle 1 voltage profiles for Figures 2C and D are shown in Figures S2 and 3.

4.4 mA/g to 96.9% at 88 mA/g (Fig 2B). Variations in the Coulombic efficiency and voltage plateaus imply the reduction/oxidation mechanism of the electrode is rate dependent.

XPS evaluated the reactions causing additional capacity delivered during the first cycle via evidence of electrolyte decomposition and $[Re_6Se_8]^{2+}$ redox activity. In Figure S5, the binding energy from 0 – 700 eV is shown for a pristine $Re_6Se_8Cl_2$ electrode and an electrode that was electrochemically reduced to 1.0 V. The most striking feature is the dramatic increase in the O (1s) intensity after the electrode is reduced compared to the pristine electrode. Upon further analysis of this region (Fig. 3A) this increase in intensity is largely from the C-O contribution at 534. 2 eV with an additional peak forming at 532.4 eV that can be attributed to formation of organic alkyl carbonates from reduction of the EC:DMC electrolyte.[28,29] This is further supported by the emergence of a new peak after discharge at the C (1s) region at ~287 eV (Fig. 3B) which also provides evidence of a new organic layer on the surface of the electrode. Notably, no evidence of the inorganic components of the SEI were detected, such as Li_2O or LiF, indicating that this SEI formed at 1 V vs. Li/Li+ is primarily comprised of organic components rather than inorganic lithium salts. Other C (1s) peaks can be attributed to the PVDF binder (C-F, ~290 eV) and the

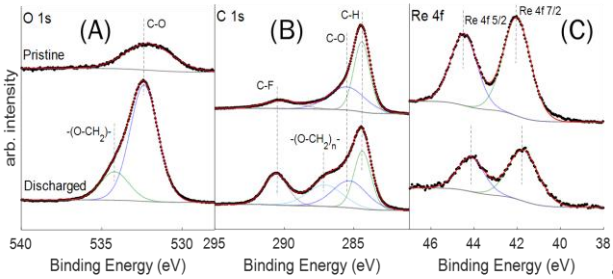

Figure 3: XPS spectrum of pristine $Re_6Se_8Cl_2$ coating and fully discharged coating with the fitted (A) O 1s region, (B) C 1s region, and (C) Re 4f region.

and 41.7 eV upon reduction as shown in Figure 3C. This shift is similar to the shifts observed in Re^{3+}/Re^{2+} oxides and indicates the Re_6 redox activity.[30]

conductive carbon additive (C-O and C-H, 284-286 eV). Additionally, there was a shift in the Re (4f 5/2) and (4f 7/2) peaks from the pristine to reduced $Re_6Se_8Cl_2$ electrode. In the pristine electrode, the Re (4f 5/2) and (4f 7/2) peaks are 44.5 and 42.0 eV, respectively; which shift to 44.1 eV.

The structural changes during the reduction and oxidation processes were studied through monitoring of the (001) plane during the first reduction and oxidation via *in situ* XRD. The rate for the *in situ* experiment was selected to provide XRD data with appropriate resolution. Figure 4 shows the voltage profile with points a-i highlighting different times during the first cycle with the corresponding (001) reflections. At the early stages of reduction the (001) reflection is indicative of a d-spacing of 8.13 Å (2θ(Cu Kα) = 10.87°), as reduction progresses to the onset of the first plateau at 1.7 V no significant change is observed. From the onset of the 1.7 V plateau to 2 ee of reduction there is a structure change as the original (001) reflection losses intensity and a new peak at d = 8.46 Å appears, coincident with a 4% lattice expansion indicative of Li^+ insertion within the interlayer space. Considering there is an emergence of a new peak rather than a peak shift, this initial insertion of Li^+ causes a new structural configuration within the material.[31,32] After 4 ee, there is a voltage drop corresponding to a contraction in the (001) plane from 8.46 to 8.38 Å. At this point the intercalation of Li^+ ions has significant impact on the structural configuration. From approximately 6 ee to the final reduction to 1.0 V there is no change to the (001) reflection showing little to no intercalation at voltages lower than 1.1 V in the interlayer spacing. The reverse process is observed upon oxidation where the lattice expansion from 8.38 back to 8.46 Å occurs between 1.75 – 2.00 V. The final phase change occurs at 2.0 V up to 3 ee where the 8.46 Å reflection loses intensity with the emergence of the original (001) reflection at 8.13 Å.

The highest irreversibility observed at a slow rate was correlated to the expansion/contraction transformation of the (001) reflection between 4-6 ee which is also associated with SEI generation. After 6 ee no additional change to the interlayer spacing was observed and was attributed to further side reactions at lower voltages. Further evidence of a lower capacity hysteresis is shown in Figure S6 where the first cycle at a faster rate of 22 mA/g monitored the (001) reflection. The same structural changes occur at the faster rate where there is a phase change followed by a lattice contraction during reduction. The final reduction capacity is less than 7 ee, providing further evidence of the rate dependency of the side reactions. At 22 mA/g there is actually a higher oxidation capacity of 3.5 ee after the first reduction compared to the

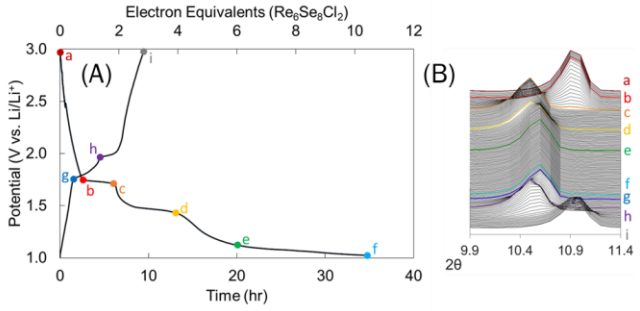

Figure 4: (A) Discharge curve at 4.4 mA/g rate from pouch cell with multiple points (a-i) highlighted. (B) *In situ* XRD data from 9.9 - 11.4° to observe the (001) reflection.

cluster bonding along with the ability of the material to intercalate Li^+ ions into the large interlayer spacing.

4.4 mA/g oxidation capacity of 2.8 ee. Showing an atypical behavior of this material to yield better reversibility at higher current due to the slow, kinetically dependent side reactions occurring at ~1 V. This electrochemical behavior is also attributed to structural integrity of the rhombic Re_2Se_2 cluster-

The robustness of the $Re_6Se_8Cl_2$ structure was tested by cycling to 2, 3, and 4 ee at the slow rate of 4.4 mA/g to investigate structural instability.[33] $Re_6Se_8Cl_2$ showed good reversibility for 50 cycles between 2 and 3 ee as shown by Figure S7A-B. However, at 4 ee, and possibly at the onset of the organic SEI formation there was significant capacity fade over 50 cycles (Fig. S7C-D). The electrodes used for this slow-cycling experiment were removed and the *ex situ* XRD patterns were collected and are shown in Figure S8. Notably, from 2-4 ee there is very little structural degradation of the parent material with only slight broadening of the (001) reflection from multiple Li^+ intercalation processes. Again, showing the robust structure provided by the Re_2Se_2 bridging found in the two dimensional layers. The *ex situ* analysis also provides evidence that the primary mechanism for capacity fade in this system is not structural degradation, but rather, formation of an organic SEI formed at voltages between 1.45-1 V showing a heightened surface reactivity.

In summary, the $Re_6Se_8Cl_2$ material was investigated as a model material for 2D cluster based systems where multi-electron transfers (2-4 ee) were demonstrated by electrochemical reduction/oxidation via Li^+ insertion/extraction across the (001) interlayer space between $[Re_6Se_8]^{2+}$ cluster frameworks.

ASSOCIATED CONTENT

Supporting Information

This material is available free of charge- http://pubs.acs.org.

Experimental methods, Cl^- structural environment, refinement results, crystal structure, XPS full scan, electrochemical profiles, *in situ* XRD (22 mA/g), *ex situ* XRD.

AUTHOR INFORMATION

Corresponding Authors

Amy C. Marschilok: amy.marschilok@stonybrook.edu
Lisa F. Szczepura: lfszcze@ilstu.edu

ORCID

Amy C. Marschilok: 0000-0001-9174-0474
Lisa F. Szczepura: 0000-0002-1464-1285
Esther S. Takeuchi: 0000-0001-8518-1047
Kenneth J. Takeuchi: 0000-0001-8518-1047

Notes

The authors declare no competing financial interests.

ACKNOWLEDGMENT

This material is based upon work supported by the National Science Foundation (NSF) (LFS, CHE RUI 1401686). Electrochemical interrogation, XRD and XPS were supported by the Center for Mesoscale Transport Properties, an Energy Frontier Research Center supported by the U.S. Department of Energy (DOE), Office of Science, award #DE-SC0012673. The XPS experiments were carried out at the Center for Functional Nanomaterials at Brookhaven National Laboratory (BNL), which is supported by the DOE, Office of Basic Energy Sciences (DE-AC02-98CH10886). Use of the National Syn-

chrotron Light Source II, (NSLSII, 28-ID) at BNL, was supported by the DOE, Office of Science, Office of Basic Energy Sciences, under Contract No. DE-SC0012704. A. M. B. acknowledges the support of the NSF Graduate Research Fellowship grant No. 1109408.

REFERENCES

1. Gao, M.-R.; Xu, Y.-F.; Jiang, J.; Yu, S.-H. Nanostructured metal chalcogenides: synthesis, modification, and applications in energy conversion and storage devices. *Chem. Soc. Rev.* **2013,** 42 (7), 2986-3017 DOI: 10.1039/C2CS35310E.

2. Alonso-Vante, N.; Schubert, B.; Tributsch, H. Transition metal cluster materials for multi-electron transfer catalysis. *Mater. Chem. Phys.* **1989,** 22 (3), 281-307 DOI: https://doi.org/10.1016/0254-0584(89)90002-3.

3. Choi, W.; Choudhary, N.; Han, G. H.; Park, J.; Akinwande, D.; Lee, Y. H. Recent development of two-dimensional transition metal dichalcogenides and their applications. *Mater. Today* **2017,** 20 (3), 116-130 DOI: https://doi.org/10.1016/j.mattod.2016.10.002.

4. Gabriel, J.-C. P.; Boubekeur, K.; Uriel, S.; Batail, P. Chemistry of Hexanuclear Rhenium Chalcohalide Clusters. *Chem. Rev.* **2001,** 101 (7), 2037-2066 DOI: 10.1021/cr980058k.

5. Durham, J. L.; Wilson, W. B.; Huh, D. N.; McDonald, R.; Szczepura, L. F. Organometallic rhenium(iii) chalcogenide clusters: coordination of N-heterocyclic carbenes. *Chem. Comm.* **2015,** 51 (52), 10536-10538 DOI: 10.1039/C5CC03215F.

6. Roland, B. K.; Flora, W. H.; Selby, H. D.; Armstrong, N. R.; Zheng, Z. Dendritic Arrays of $[Re_6(\mu_3\text{-}Se)_8]^{2+}$ Core-Containing Clusters: Exploratory Synthesis and Electrochemical Studies. *J. Am. Chem. Soc.* **2006,** 128 (20), 6620-6625 DOI: 10.1021/ja057548w.

7. Sokolov, M. N.; Mikhailov, M. A.; Brylev, K. A.; Virovets, A. V.; Vicent, C.; Kompankov, N. B.; Kitamura, N.; Fedin, V. P. Alkynyl Complexes of High-Valence Clusters. Synthesis and Luminescence Properties of $[Mo_6I_8(C{\equiv}CC(O)OMe)_6]^{2-}$, the First Complex with Exclusively Organometallic Outer Ligands in the Family of Octahedral $\{M_6X_8\}$ Clusters. *Inorg. Chem.* **2013,** 52 (21), 12477-12481 DOI: 10.1021/ic401377g.

8. Gray, T. G.; Rudzinski, C. M.; Meyer, E. E.; Holm, R. H.; Nocera, D. G. Spectroscopic and photophysical properties of hexanuclear rhenium (III) chalcogenide clusters. *J. Am. Chem. Soc.* **2003,** (125), 4755-4770.

9. Rabanal-León, W. A.; Murillo-López, J. A.; Páez-Hernández, D.; Arratia-Pérez, R. Understanding the Influence of Terminal Ligands on the Electronic Structure and Bonding Nature in $[Re_6(\mu_3\text{-}Q_8)]^{2+}$ Clusters. *J. Phys. Chem. A* **2014,** 118 (46), 11083-11089 DOI: 10.1021/jp508892r.

10. Wilson, W. B.; Stark, K.; Johnson, D. B.; Ren, Y.; Ishida, H.; Cedeño, D. L.; Szczepura, L. F. Photophysical Properties of a Series of Rhenium Selenide Cluster Complexes Containing Nitrogen-Donor Ligands. *Eur. J. Inorg. Chem.* **2014,** 2014 (13), 2254-2261 DOI: 10.1002/ejic.201301626.

11. Yoshimura, T.; Suo, C.; Tsuge, K.; Ishizaka, S.; Nozaki, K.; Sasaki, Y.; Kitamura, N.; Shinohara, A. Excited-State Properties of Octahedral Hexarhenium(III) Complexes with Redox-active N-heteroaromatic Ligands. *Inorg. Chem.* **2010,** 49 (2), 531-540 DOI: 10.1021/ic9015788.

12. Kirakci, K.; Kubat, P.; Langmaier, J.; Polivka, T.; Fuciman, M.; Fejfarova, K.; Lang, K. A comparative study of the redox and excited state properties of $(nBu_4N)_2[Mo_6X_{14}]$ and $(nBu_4N)_2[Mo_6X_8(CF_3COO)_6]$ (X = Cl, Br, or I). *Dalton Trans.* **2013,** 42 (19), 7224-7232 DOI: 10.1039/C3DT32863E.

13. Guilbaud, C.; Deluzet, A.; Domercq, B.; Molinie, P.; Boubekeur, K.; Batail, P.; Coulon, C. $(NBu^n{}_4{}^+)_3[Re_6S_8Cl_6]^{3-}$: synthesis and luminescence of the paramagnetic, open shell member of a hexanuclear chalcohalide cluster redox system. *Chem. Comm.* **1999,** (18), 1867-1868 DOI: 10.1039/A904669K.

14. Cordier, S.; Molard, Y.; Brylev, K. A.; Mironov, Y. V.; Grasset, F.; Fabre, B.; Naumov, N. G. Advances in the Engineering of Near Infrared Emitting Liquid Crystals and Copolymers, Extended Porous Frameworks, Theranostic Tools and Molecular Junctions Using Tailored Re_6 Cluster Building Blocks. *J. Clust. Sci.* **2015,** 26 (1), 53-81 DOI: 10.1007/s10876-014-0734-0.

15. Amela-Cortes, M.; Cordier, S.; Naumov, N. G.; Meriadec, C.; Artzner, F.; Molard, Y. Hexacyano octahedral metallic clusters as versatile building blocks in the design of extended polymeric framework and clustomesogens. *J. Mater. Chem. C* **2014,** 2 (46), 9813-9823 DOI: 10.1039/C4TC02098G.

16. Tulsky, E. G.; Crawford, N. R. M.; Baudron, S. A.; Batail, P.; Long, J. R. Cluster-to-Metal Magnetic Coupling: Synthesis and Characterization of 25-Electron $[Re_{6\text{-}n}Os_nSe_8(CN)_6]^{(5\text{-}n)\text{-}}$ (n = 1, 2) Clusters and $\{Re_{6\text{-}n}Os_nSe_8[CNCu(Me_6tren)]_6\}^{9+}$ (n = 0, 1, 2) Assemblies. *J. Am. Chem. Soc.* **2003,** 125 (50), 15543-15553 DOI: 10.1021/ja037444q.

17. Litvinova, Y. M.; Gayfulin, Y. M.; Kovalenko, K. A.; Samsonenko, D. G.; van Leusen, J.; Korolkov, I. V.; Fedin, V. P.; Mironov, Y. V. Multifunctional Metal–Organic Frameworks Based on Redox-Active Rhenium Octahedral Clusters. *Inorg. Chem.* **2018**, DOI: 10.1021/acs.inorgchem.7b02974.

18. Carlsson, S.; Zorina, L.; Allan, D. R.; Attfield, J. P.; Canadell, E.; Batail, P. Robust Dirac-Cone Band Structure in the Molecular Kagome Compound $(EDT\text{-}TTF\text{-}CONH_2)_6[Re_6Se_8(CN)_6]$. *Inorg. Chem.* **2013,** 52 (6), 3326-3333 DOI: 10.1021/ic302790m.

19. Welch, E. J.; Long, J. R. Atomlike Building Units of Adjustable Character: Solid-State and Solution Routes to Manipulating Hexanuclear Transition Metal Chalcohalide Clusters. *Prog. Inorg. Chem.*; John Wiley & Sons, Inc.: 2005; pp 1-45.

20. Cho, J.-H.; Aykol, M.; Kim, S.; Ha, J.-H.; Wolverton, C.; Chung, K. Y.; Kim, K.-B.; Cho, B.-W. Controlling the Intercalation Chemistry to Design High-Performance Dual-Salt Hybrid Rechargeable Batteries. *J. Am. Chem. Soc.* **2014,** 136 (46), 16116-16119 DOI: 10.1021/ja5084632.

21. Richard, J.; Benayad, A.; Colin, J. F.; Martinet, S. Charge Transfer Mechanism into the Chevrel Phase Mo_6S_8 during Mg Intercalation. *J. Phys. Chem. C* **2017,** 121 (32), 17096-17103 DOI: 10.1021/acs.jpcc.7b03979.

22. Thole, F.; Wan, L. F.; Prendergast, D. Re-examining the Chevrel phase Mo_6S_8 cathode for Mg intercalation from an electronic structure perspective. *Phys. Chem. Chem. Phys.* **2015,** 17 (35), 22548-22551 DOI: 10.1039/C5CP03046C.

23. Long, J. R.; Williamson, A. S.; Holm, R. H. Dimensional reduction of $Re_6Se_8Cl_2$: sheets, chains, and discrete clusters composed of chloride-terminated $[Re_6Q_8]^{2+}$ (Q = S, Se) cores. *Angew. Chem., Int. Ed. Engl.* **1995,** 34 (2), 226-9 DOI: 10.1002/anie.199502261.

24. Long, J. R.; McCarty, L. S.; Holm, R. H. A Solid-State Route to Molecular Clusters: Access to the Solution Chemistry of $[Re_6Q_8]^{2+}$ (Q = S, Se) Core-Containing Clusters via Dimensional Reduction. *J. Am. Chem. Soc.* **1996,** 118 (19), 4603-16 DOI: 10.1021/JA960216U.

25. Perrin, A.; Perrin, C. Low-Dimensional Frameworks in Solid State Chemistry of Mo_6 and Re_6 Cluster Chalcohalides. *Eur. J. Inorg. Chem.* **2011,** 2011 (26), 3848-3856 DOI: 10.1002/ejic.201100400.

26. Leduc, L.; Padiou, J.; Perrin, A.; Sergent, M. Synthèse et caractérisation d'un nouveau chalcohalogénure à clusters octaédriques de rhénium à caractère bidimensionnel: $Re_6Se_8Cl_2$. *J. Less Common Met.* **1983,** 95 (1), 73-80 DOI: https://doi.org/10.1016/0022-5088(83)90385-5.

27. Peled, E.; Menkin, S. Review—SEI: Past, Present and Future. *J. Electrochem. Soc.* **2017,** 164 (7), A1703-A1719 DOI: 10.1149/2.1441707jes.

28. Dalavi, S.; Guduru, P.; Lucht, B. L. Performance Enhancing Electrolyte Additives for Lithium Ion Batteries with Silicon Anodes. *J. Electrochem. Soc.* **2012,** 159 (5), A642-A646 DOI: 10.1149/2.076205jes.

29. An, S. J.; Li, J.; Daniel, C.; Mohanty, D.; Nagpure, S.; Wood, D. L. The state of understanding of the lithium-ion-battery graphite solid electrolyte interphase (SEI) and its relationship to formation cycling. *Carbon* **2016,** 105 , 52-76 DOI: https://doi.org/10.1016/j.carbon.2016.04.008.

30. Okal, J.; Tylus, W.; Kępiński, L. XPS study of oxidation of rhenium metal on $\gamma\text{-}Al_2O_3$ support. *J. Catal.* **2004,** 225 (2), 498-509 DOI: https://doi.org/10.1016/j.jcat.2004.05.004.

31. Zhang, Q.; Brady, A. B.; Pelliccione, C. J.; Bock, D. C.; Bruck, A. M.; Li, J.; Sarbada, V.; Hull, R.; Stach, E. A.; Takeuchi, K. J.; Takeuchi, E. S.; Liu, P.; Marschilok, A. C. Investigation of Structural Evolution of $Li_{1.1}V_3O_8$ by In Situ X-ray Diffraction and Density Functional Theory Calculations. *Chem. Mater.* **2017,** 29 (5), 2364-2373 DOI: 10.1021/acs.chemmater.7b00096.
32. Cavoué, T.; Emery, N.; Umirov, N.; Bach, S.; Berger, P.; Bakenov, Z.; Cénac-Morthe, C.; Pereira-Ramos, J.-P. $Li_{2.0}Ni_{0.67}N$, a Promising Negative Electrode Material for Li-Ion Batteries with a Soft Structural Response. *Inorg. Chem.* **2017,** 56 (22), 13815-13821 DOI: 10.1021/acs.inorgchem.7b01903.
33. Levi, E.; Aurbach, D. Lattice Strains in the Ligand Framework in the Octahedral Metal Cluster Compounds as the Origin of their Instability. *Chem. Mater.* **2011,** 23 (7), 1901-1914 DOI: 10.1021/cm103617e.

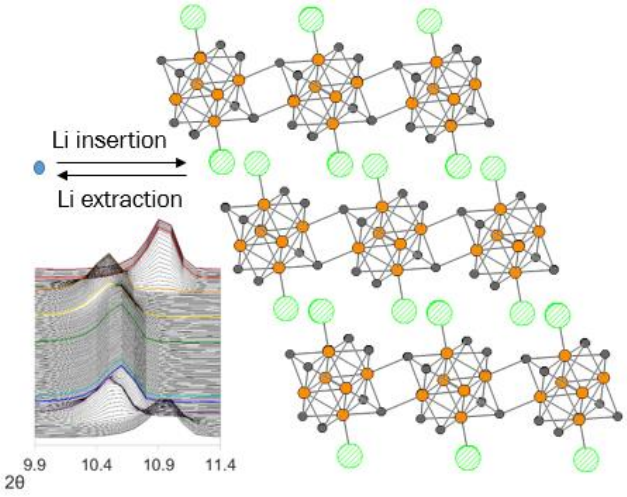

The ability of cluster-based $Re_6Se_8Cl_2$ to be used for electrochemical energy storage is demonstrated, showing structural stability and high rate capability.

Reversible Electrochemical Lithium Ion Insertion into the Rhenium Cluster Chalcogenide-Halide, $Re_6Se_8Cl_2$

Andrea M. Bruck[†], Jiefu Yin[†], Xiao Tong[‡], Esther S. Takeuchi[†,‖,|], Kenneth J. Takeuchi[†,‖], Lisa F. Szczepura[§,*], Amy C. Marschilok[†,‖,*]

[†]Department of Chemistry, Stony Brook University, Stony Brook, NY 11794, USA

[‡]Center for Functional Nanomaterials, Brookhaven National Laboratory, Upton, NY 11973, USA

[‖]Department of Materials Science and Engineering, Stony Brook University, Stony Brook, NY 11794, USA

[|]Energy Sciences Directorate, Brookhaven National Laboratory, Upton, NY 11973, USA

[§]Department of Chemistry, Illinois State University, Normal, IL, 61790-4160, USA

***corresponding authors:** (LFS) lfszcze@ilstu.edu; (ACM) amy.marschilok@stonybrook.edu

Supplemental Information

Experimental

Materials Synthesis: $Re_6Se_8Cl_2$ was prepared using a modification of the previously published procedure.[1] Rhenium (Alfa Aesar, 99.5%, -325 mesh), rhenium(V) chloride (CERAC, 99.9%, -40 mesh) and selenium (Sigma Aldrich, 99.5%, -100 mesh) were combined in near-stoichiometric amounts inside an inert atmosphere glove box (a 10% excess of Re and $ReCl_5$ was utilized). The solids were ground into a fine powder with a mortar and pestle and then placed in a fused silica tube. The tube was stoppered, brought out of the glove box and immediately sealed under vacuum. The tube was then heated in a tube furnace at 1050°C (ramp rate of 3°C/min) for 24 hours then cooled back to room temperature. The resulting product, which was a fine black powder, was handled in air. The material was stored in air for >40 days prior to the synchrotron-based x-ray diffraction (XRD) measurement and for >4 months prior to the *in situ* lab based XRD.

Materials Characterization: The $Re_6Se_8Cl_2$ powder was packed in a polyimide tube for X-ray Powder Diffraction (XPD) measurements at Brookhaven National Laboratories (BNL) National Synchrotron Light Source II (NSLS-II) beamline 28-ID. The beam was calibrated to a wavelength of 0.1832 Å and used a 16-inch CsI scintillator detector for the collection of 2D images that were integrated to 1D diffraction data using a LaB_6 standard. Rietveld refinements of the collected patterns were performed using the GSASII software.[2] X-ray Photoelectron Spectroscopy (XPS) measurements were carried out at BNL's Center for Functional Nanomaterials (CFN) in UHV chamber equipped with a Phoibos 100 MCD analyzer and a non-monochromatized Mg-Kα X-ray source. Coatings were measured in the pristine state of removed from the cell after discharge and stored in an Argon filled glovebox until the measurement was taken in vacuum. Therefore, we assume minimal air exposure to the sample and contribute the change in O(1s) signal to SEI. Charging effects were corrected by adjusting the binding energy of C (1s) peak to 284.4 eV.

Electrochemical testing: The $Re_6Se_8Cl_2$ electrodes were constructed by mixing 70wt% $Re_6Se_8Cl_2$, 20wt% acetylene black carbon, and 10wt% polyvinylidene difluoride (PVDF) binder. The mixture was cast onto Al foil as a slurry where the materials were suspended in n-methyl-2-pyrrolidone (NMP) and dried prior to use. Two electrode coin type cells were assembled in an $Ar_{(g)}$ filled glovebox using a Li metal counter electrode and a 1 M $LiPF_6$ in 3:7 ethylene carbonate (EC): dimethylcarbonate (DMC) electrolyte. During

cyclic voltammetry (CV) the cells were scanned at a rate of 0.01 mV/s at room temperature on a Bio-Logic Science Instruments EC instrument. Rate capability and extended cycling tests were performed galvonastatically using a MACCOR battery tester with a 1.00 or 1.45 V cut-off voltage. *In situ* XRD during reduction and oxidation was conducted as previously described.[3] Briefly, specially designed pouch cells were assembled using Li metal, polyethylene separator, 1 M $LiPF_6$ in 3:7 EC:DMC (v/v) electrolyte, and the aforementioned $Re_6Se_8Cl_2$ electrodes. XRD scans were continuously collected with a 0.1º step size at a scan rate of 2º/min by a Rigaku Mini-Flex X-ray powder diffractometer during reduction and oxidation using a Bio-Logic Science Instruments EC.

Supplemental Tables and Figures

Parameter		**Value**
Space group		P-1
Symmetry		triclinic
Unit cell	a, Å	6.5908(2)
	b, Å	6.6279(2)
	c, Å	9.0643(4)
	α,º	100.149(5)
	β,º	113.507(5)
	γ,º	93.654(5)
Re1	x	0.56999(3)
	y	0.7548(4)
	z	0.4653(2)
	Uiso	0.001(1)
Re2	x	0.1977(5)
	y	0.5377(5)
	z	0.4311(3)
	Uiso	0.009(1)
Re3	x	0.5565(5)
	y	0.6258(4)
	z	0.7161(3)
	Uiso	0.0011(9)
Se1	x	0.907(1)
	y	0.832(1)
	z	0.732(1)
	Uiso	0.012(2)
Se2	x	0.221(1)
	y	0.6610(9)
	z	0.1909(9)
	Uiso	0.009(2)
Se3	x	0.785(1)
	y	0.598(1)
	z	0.3080(8)
	Uiso	0.001(1)

Se4	x	0.676(1)
	y	0.0974(4)
	z	0.3903(9)
	Uiso	0.007(2)
Cl1	x	0.646(2)
	y	0.780(2)
	z	0.995(2)
	Uiso	0.024(5)
Crystallite size	Uniaxial, nm	642 ± 91
	Axial, nm	1060 ± 180
Microstrain, %		0.29(1)
wR, %		7.93
GOF		1.91

Table S1: Refined crystallographic parameters of the pristine $Re_6Se_8Cl_2$ material.

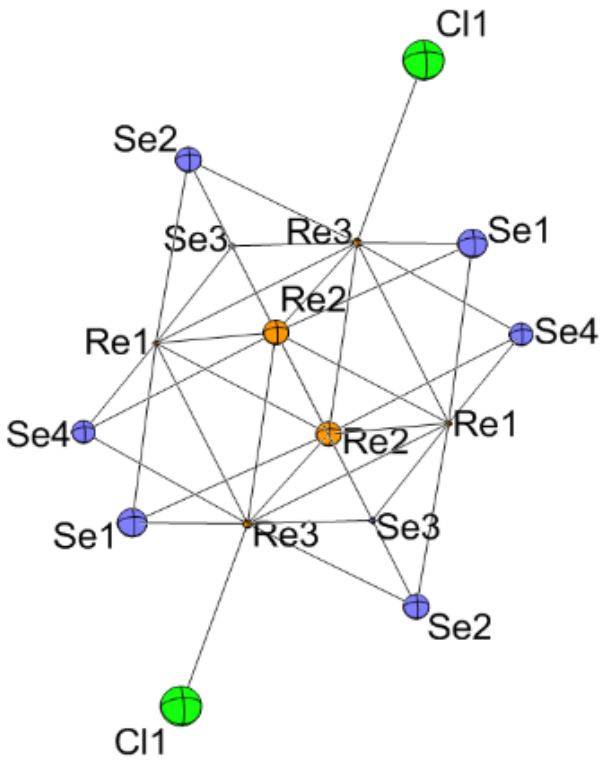

Figure S1: Thermal ellipsoids of the refined unit cell of $Re_6Se_8Cl_2$.

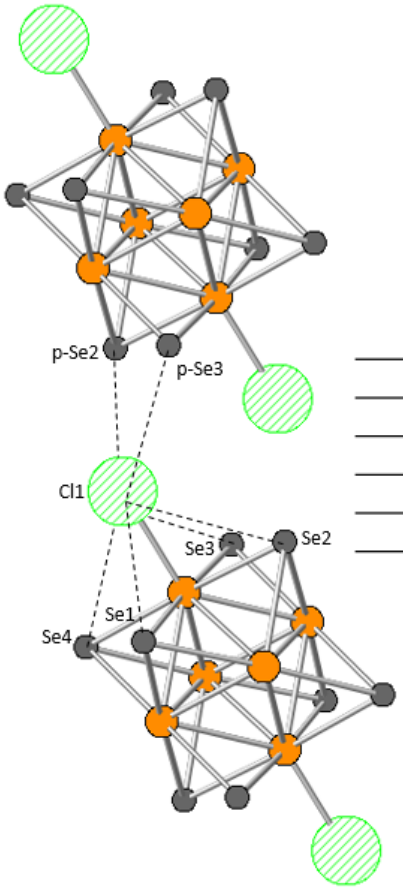

	Atomic distance (Å)
Se1-Cl1	3.501
Se2-Cl1	3.456
Se3-Cl1	3.518
Se4-Cl1	3.561
p-Se2-Cl1	3.969
p-Se3-Cl1	3.099

Figure S2: Schematic and table corresponding to the Se-Cl atom distances in the interlayer spacing where the p-Se atoms represent the Se atoms in the parallel Re_6Se_8 stack.

Within the interlayer the closest Cl···Cl distance is 3.593 Å compared to the Re-Cl bond distance of 2.372 Å and the Se···Cl that vary from approximately 3-4 Å. In the Se···Cl bonding there are four distinct Se atoms pertaining to the four distinct bond distances in the unit cell as shown in Figure S2. The Se-Cl distances from the adjoining cluster are all approximately 3.5 Å where the nearest Se···Cl distance from a parallel cluster is 3.099 Å which would be the closest non-bonding atom in proximity to the terminal Cl^-.

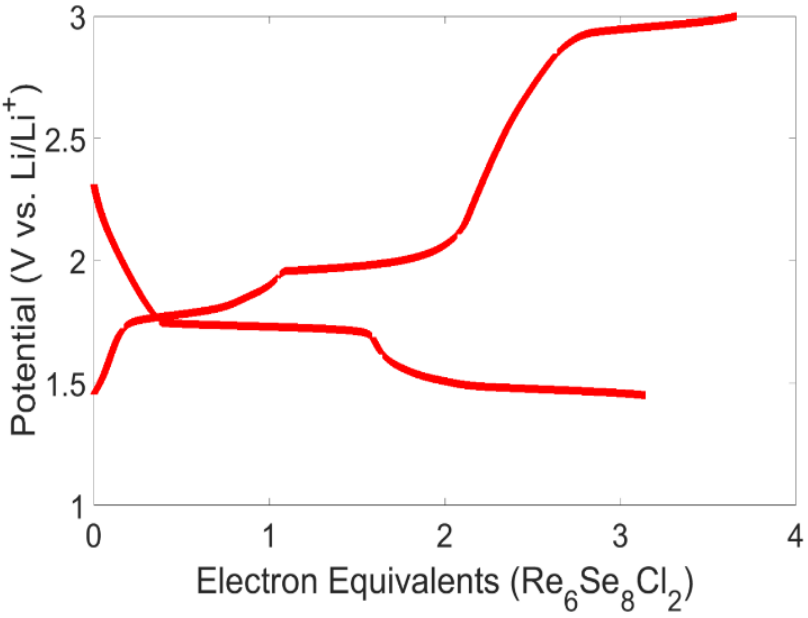

Figure S3: First cycle of the $Li/Re_6Se_8Cl_2$ electrochemical cell to 1.45 V. Voltage profiles for subsequent cycles are shown in Figure 2C.

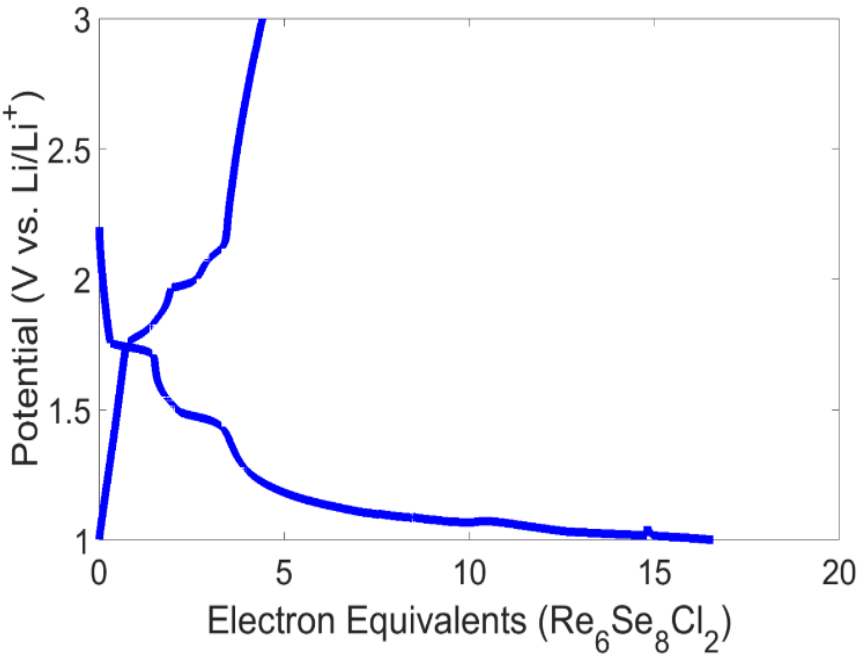

Figure S4: First cycle of the Li/$Re_6Se_8Cl_2$ electrochemical cell to 1 V. Voltage profiles for subsequent cycles are shown in Figure 2D.

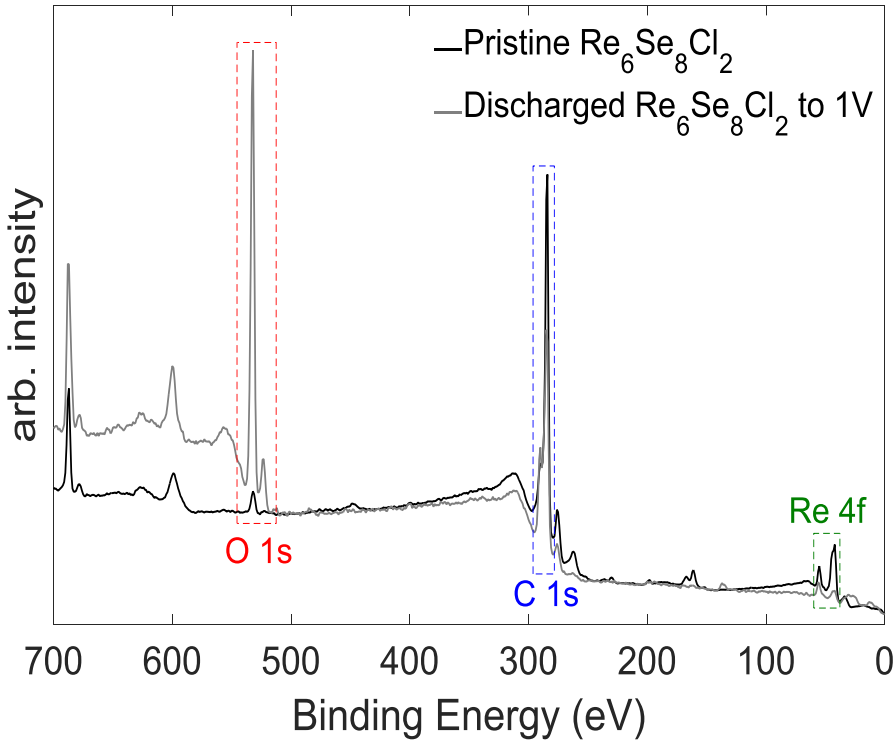

Figure S5: XPS spectrum of pristine $Re_6Se_8Cl_2$ coating and fully discharged coating full scan.

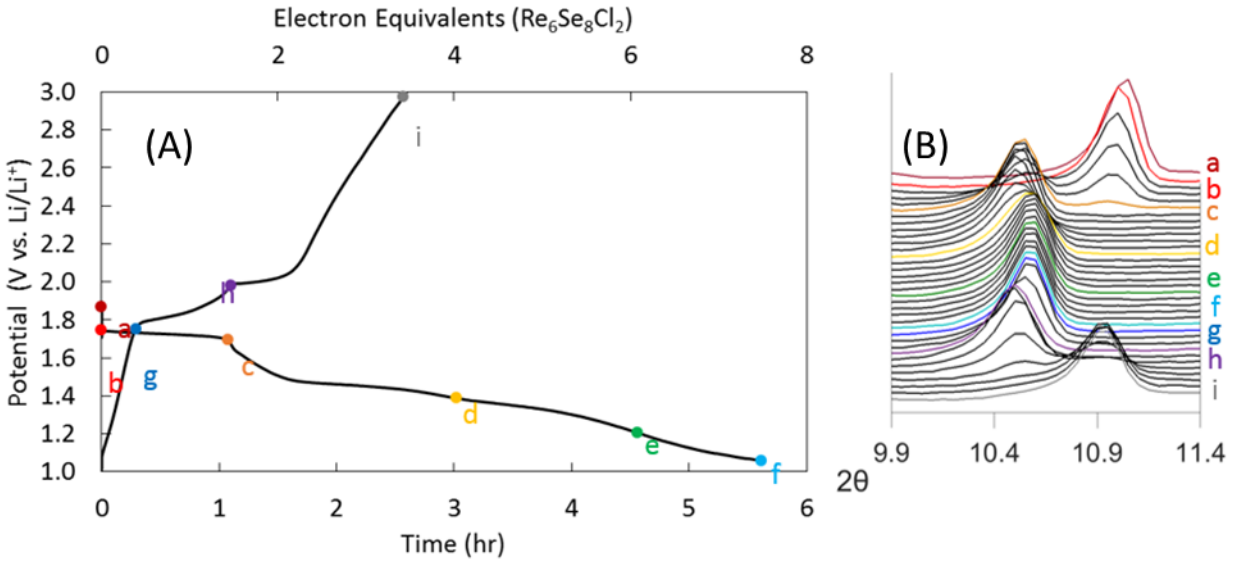

Figure S6: (A) First cycle at 22 mA/g from Li/$Re_6Se_8Cl_2$ pouch-type electrochemical cell with multiple points (a-i) highlighted. (B) *In situ* XRD data from 9.9 - 11.4º to observe the (001) reflection. Various points from the discharge curve corresponding to certain patterns were highlighted (a-i).

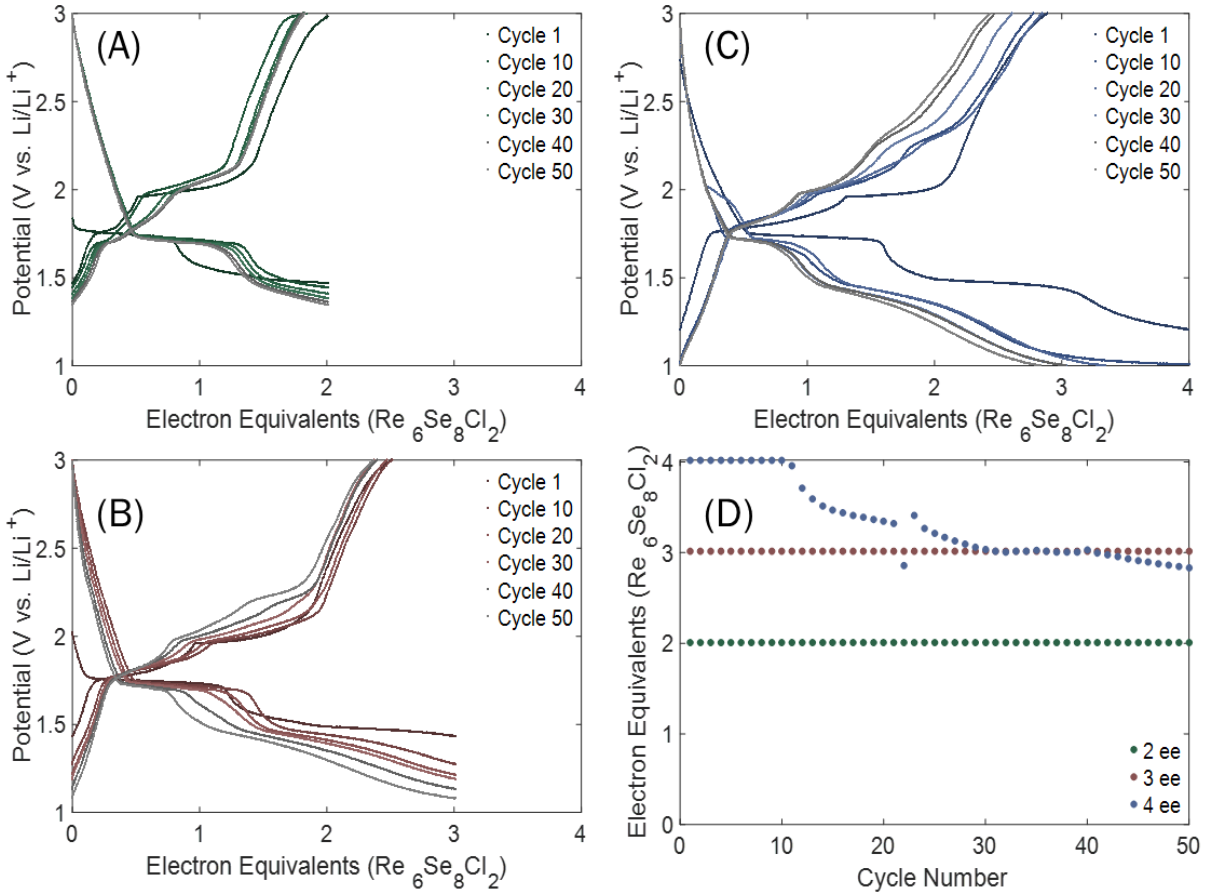

Figure S7: $Li/Re_6Se_8Cl_2$ coin-type electrochemical cell cycle profiles when (A) cycled at 2 ee (B) cycled at 3 ee (C) cycled at 4 ee , and (D) the discharge capacity in ee over 50 cycles for the 3 conditions.

When the material was cycled to 2 and 3 ee over 50 cycles at a slow rate of 4.4 mAg/g we observed a sustained reversibility with some voltage decay in the 3 ee cycling. Upon cycling 4 ee more significant fade (2.8 ee discharge capacity at cycle 50) was observed consistent with the voltage where SEI formation onset is expected.

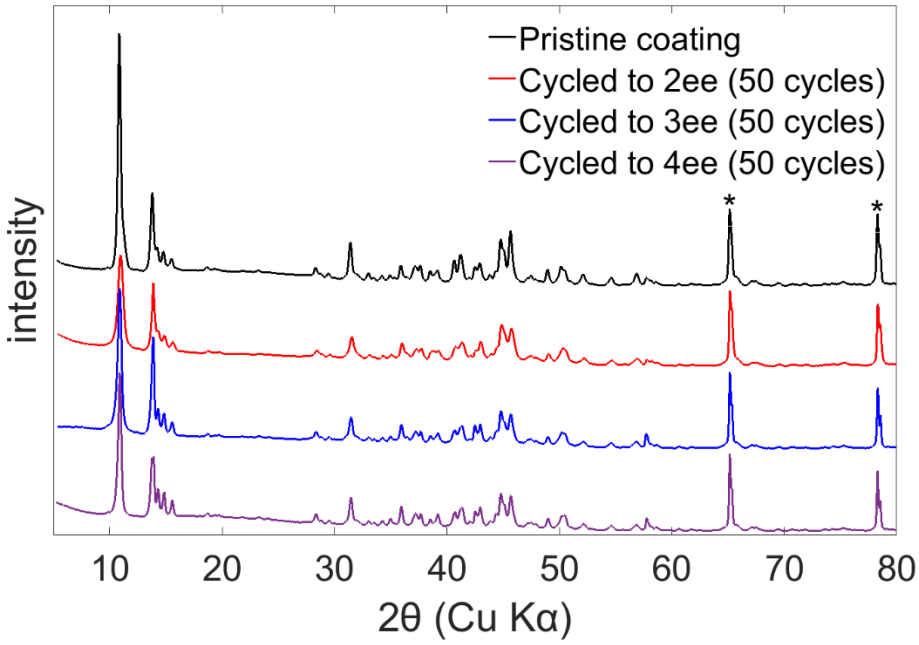

Figure S8: *Ex situ* XRD patterns of $Re_6Se_8Cl_2$ based electrodes cycled to various electron equivalents and recovered in the charged state after 50 cycles. '*' represent reflections from the Al foil substrate.

References

1. Leduc, L.; Padiou, J.; Perrin, A.; Sergent, M. Synthèse et caractérisation d'un nouveau chalcohalogénure à clusters octaédriques de rhénium à caractère bidimensionnel: $Re_6Se_8Cl_2$. *J. Less Common Met.* **1983,** 95 (1), 73-80 DOI: https://doi.org/10.1016/0022-5088(83)90385-5.

2. Toby, B. H.; Von Dreele, R. B. GSAS-II: the genesis of a modern open-source all purpose crystallography software package. *J. App. Crystal.* **2013,** 46, 544-549 DOI: 10.1107/s0021889813003531.

3. Bock, D. C.; Pelliccione, C. J.; Zhang, W.; Timoshenko, J.; Knehr, K. W.; West, A. C.; Wang, F.; Li, Y.; Frenkel, A. I.; Takeuchi, E. S.; Takeuchi, K. J.; Marschilok, A. C. Size dependent behavior of Fe_3O_4 crystals during electrochemical (de)lithiation: an in situ X-ray diffraction, ex situ X-ray absorption spectroscopy, transmission electron microscopy and theoretical investigation. *Phys. Chem. Chem. Phys.* **2017,** 19 (31), 20867-20880 DOI: 10.1039/C7CP03312E.